Acta Crystallographica Section D
Biological Crystallography
ISSN 0907-4449

Crystallographic titration of cubic insulin crystals: pH affects Glu*B*13 switching and sulfate binding

Jiasheng Diao†

Institute of Molecular Biophysics, Florida State University, Tallahassee, Florida 32306, USA

† Present address: Department of Biological Sciences, Purdue University, West Lafayette, Indiana 47907, USA.

Correspondence e-mail: diao@bilbo.bio.purdue.edu

Received 13 August 2002
Accepted 24 January 2003

PDB References: cubic insulin, pH 5.00, 1b17, r1b17sf; pH 5.53, 1b18, r1b18sf; pH 5.80, 1b19, r1b19sf; pH 6.00, 1b2a, r1b2asf; pH 6.16, 1b2b, r1b2bsf; pH 6.26, 1b2c, r1b2csf; pH 6.35, 1b2d, r1b2dsf; pH 6.50, 1b2e, r1b2esf; pH 6.98, 1b2f, r1b2fsf; pH 9.00, 1b2g, r1b2gsf.

Structures of porcine insulin crystals soaked in 1 *M* sodium sulfate at pH 5.00, 5.53, 5.80, 6.00, 6.16, 6.26, 6.35, 6.50, 6.98 and 9.00 have been determined at between 1.7 and 1.9 Å resolution. Glu*B*13 exhibits a single conformation at pH $\leq$ 5.80, two conformations between pH 6.00 and 6.98 and a single conformation at pH 9.00. Between pH 6.00 and 6.98, the conformation of Glu*B*13 switches from one rotamer to another rotamer. Between pH 6.16 and 6.26, Phe*B*1 undergoes a significant conformational change. By pH 9.00 many residues have undergone relatively large shifts and His*B*10 exhibits a double conformation. As a result of the pH increase, the occupancy of the sulfate ion decreases from a maximum of 1.00 at pH 5.00 to a minimum of 0.46 at pH 6.50. Comparison of the structures, the observed and calculated structure factors and map correlation coefficients indicate that the porcine insulin structure changes gradually as a function of pH.

1. Introduction

The cubic insulin crystal structure (space group $I2_13$, unit-cell parameter 78.9 Å, solvent content 65%) has previously been solved by the molecular-replacement method (Dodson *et al.*, 1978) and refined to 1.7 Å with an *R* factor of 17.3% (Badger *et al.*, 1991). Studies of cubic insulin crystals have focused on analyzing the effects of changing several different conditions such as pH, ionic strength, ionic composition and water activity. Several structures of cubic insulin crystals have been compared across a broad range of conditions, for example, from crystals in various 0.1 *M* sodium salt solutions in the pH range 7–10 (Gursky *et al.*, 1992), in 1 *M* Na_2SO_4 pH 5–11 (Gursky *et al.*, 1994), in carbonate solutions containing a wide range of different monovalent cations at pH 9.5–10 (Badger *et al.*, 1994) and also from crystals in 2 *M* glucose (Yu & Caspar, 1998). The cubic insulin structure remained remarkably stable and relatively unchanged under all these conditions; in cases where conformational changes significantly displaced the positions of several protein atoms, the majority of the insulin molecule and crystal lattice remained undisturbed.

In a study of stereospecific dihaloalkane binding in cubic insulin crystals (Gursky *et al.*, 1994), it was observed that a structural transition of Glu*B*13 occurred as a result of lowering the pH from 9.00 to 5.00 in 1 *M* Na_2SO_4 and that sulfate ions were bound by rearranged *B*1 NH_3^+ groups. The observation resulted from two structures at pH 5.00 and 9.00. To explore the structural transition process, we have now determined ten structures between pH 5.00 and 9.00. The crystallographic titration of cubic insulin crystals will demonstrate whether there is an intermediate in the structural transition process.

This study will increase our understanding of pH effects on dynamic movement of the polar groups of biomacromolecules and on ion binding to biomacromolecules.

2. Materials and methods

2.1. Crystallization

Porcine insulin was purchased from Sigma (St Louis, MO, USA). Crystals were grown by the dialysis method at room temperature (Gursky *et al.*, 1992; Dodson *et al.*, 1978). Porcine insulin was dissolved in 0.05 *M* Na_2HPO_4, 0.001 *M* Na_2EDTA pH 11 to a protein concentration of 18 mg ml^{-1}. The protein solution was kept at room temperature for 2 h for the porcine insulin to completely dissolve. 3–4 dialysis buttons (35 µl), filled with the protein solution and sealed with dialysis membrane (1000 Da molecular-weight cutoff), were placed in a jar containing 20 ml dialysis solution consisting of 0.15 *M* Na_2HPO_4, 0.001 *M* Na_2EDTA pH 9.2. After 24 h, 3–5 ml of 0.7 *M* Na_2HPO_4 (pH 8.9–9.0) was added to the dialysis solution to increase the dialysis salt concentration. After a few days, crystals grew to dimensions of 1 × 1 × 1 mm.

The crystals were soaked in 1 *M* Na_2SO_4 and at different pH values, buffered by buffer systems of different buffering ranges: 50 m*M* sodium acetate at pH 5.00, 50 m*M* sodium citrate at pH 5.53, 5.80, 6.00, 6.16, 6.26 and 6.35, 50 m*M* sodium cacodylate at pH 6.50 and 6.98 and 50 m*M* Tris–HCl at pH 9.00. Crystals soaked in 1 *M* Na_2SO_4 and at different pH values were mounted in a capillary for data collection at room temperature.

Table 1
Crystallographic statistics for cubic insulin crystals at ten different pH values.

pH	5.00	5.53	5.80	6.00	6.16	6.26	6.35	6.50	6.98	9.00
Data resolution (Å)	1.7	1.8	1.8	1.7	1.8	1.8	1.7	1.9	1.9	1.8
Data completeness (%)	99.25	99.70	99.66	98.43	95.24	94.87	99.40	99.86	99.92	94.85
R_{sym}† (%)	8.3	9.4	10.4	12.4	4.6	7.7	8.6	7.4	6.0	6.5
Unit-cell parameter (Å)	78.71	78.72	78.73	78.75	78.70	78.78	78.81	78.74	78.77	78.87
R factor‡ (%)	18.50	18.39	19.06	18.79	19.30	18.69	19.40	19.27	18.79	20.23
R_{free}‡ (%)	21.99	21.73	22.97	23.00	22.77	21.93	22.99	22.91	24.32	22.40
R.m.s.d.										
Bond lengths (Å)	0.006	0.006	0.006	0.006	0.006	0.006	0.006	0.006	0.006	0.006
Bond angles (°)	1.16	1.14	1.13	1.12	1.17	1.14	1.11	1.17	1.10	1.15
B factors										
Averaged main chain	16.29	15.88	16.81	16.69	18.79	16.96	17.78	20.10	21.37	18.32
R.m.s.d.	0.77	0.78	0.82	0.78	0.80	0.84	0.74	0.88	0.93	0.84
Averaged side chain	19.01	18.46	19.51	19.18	21.19	19.52	20.01	22.31	23.88	21.02
R.m.s.d.	1.22	1.16	1.18	1.16	1.11	1.20	1.08	1.13	1.29	1.25
Water molecules										
Number	75	64	59	67	66	65	69	56	66	49
Average *B* factor	49.66	47.47	48.29	50.11	57.39	50.84	51.35	53.74	58.42	48.34
R.m.s.d.	18.80	18.70	16.63	17.55	20.32	18.68	18.27	19.98	21.13	16.92

† All R_{sym} values except for that at pH 6.98 (1.9 Å) were calculated using data to 1.7 Å resolution. Owing to high R_{sym} values in high-resolution shells, the actual high resolution used in the refinement (see row 1) is not always 1.7 Å. The low resolution used in the refinement is 10 Å. ‡ *R* factors and R_{free} values were calculated using the data between 10 Å and the corresponding high resolution listed in the first row.

2.2. Data collection and reduction

Diffraction data were collected with an R-AXIS IIc image-plate detector using Cu *Kα* radiation from a Rigaku RU-200 rotating-anode generator. The X-ray generator was operated at 40 kV and 90 mA, the swing angle of the detector was 16.2° and the detector distance was 125 mm. Normally, 30 frames of diffraction data were collected with an oscillation range of 2° and an exposure time of 60 min. The intensities were integrated and scaled using *DENZO* and *SCALEPACK* (Otwinowski & Minor, 1997) and were converted to amplitudes using *TRUNCATE* (French & Wilson, 1978) from the *CCP*4 suite (Collaborative Computational Project, Number 4, 1994). The data-collection statistics of all data sets are presented in Table 1.

2.3. Structure determination and refinement

The porcine insulin structure (Badger *et al.*, 1991; PDB code 9ins) was used as the starting model. 10% of the diffraction data were removed as a test data set to calculate the free *R* factor. Conventional positional refinement was applied (Brünger, 1992). After the first round of refinement using data in the resolution range 10–2.5 Å, the resolution was extended to 2.2, 2.0 Å and to the highest resolution in a stepwise manner. Manual building using *O* (Jones *et al.*, 1991) and refinement were carried out during each resolution extension. Individual *B*-factor refinement was initiated at 2.0 Å and water molecules were added at the highest resolution of each data set. With the occupancy fixed at 0.5, the *B* factors of the double conformations of Glu*B*13 were refined. The *B* factors of the corresponding atoms of the double conformations of Glu*B*13 were then averaged and the occupancies of the double conformations of Glu*B*13 were refined. The occupancies were further used to refine new *B* factors. The *B* factors and occupancies of the double conformations of Glu*B*13 were refined alternately until convergence. The occupancy of the sulfate ion in the structure at pH 5.00 was fixed at 1.00 and the *B* factors of the sulfate ion at pH 5.00 were refined. Using the *B* factors of the sulfate ion from the structure at pH 5.00, the occupancy of the sulfate ion in all other structures was refined and obtained. The refinement statistics of all the structures are listed in Table 1.

3. Results

3.1. Crystal structures of porcine insulin at different pH values

Porcine insulin structures at different pH values resemble each other (Table 2). The superposition of all the structures shows a good fit for all residues except for Asn*A*21, Phe*B*1, Glu*B*13, Glu*B*21, Lys*B*29 and Ala*B*30 (Fig. 1). The high flexibility of the surface residue Glu*B*21 and the C-terminal residues Asn*A*21, Lys*B*29 and Ala*B*30 are common among

insulin structures. At pH 9.00 many residues have undergone relatively large shifts and His*B*10 has double conformations.

The electron-density maps at different pH values show clear density for Glu*B*13 (Fig. 2). At pH $\leq$ 5.80 Glu*B*13 exhibits a single conformation, conformation I. At between pH 6.00 and 6.98, in addition to the original conformation I, the side chain of Glu*B*13 rotates about 120° around bond CA—CB and forms a new conformation, conformation II, so that the two conformations of Glu*B*13 coexist in porcine insulin crystals (Fig. 3). At pH 9.00 Glu*B*13 exists in conformation II. The four dyad-related water molecules above Glu*B*13 (Fig. 3) also show shifts as the pH increases. As the pH increases from 5.00 to 9.00, the inner two water molecules (O34 and O34′ at pH 6.00) rotate about 45° around a crystallographic twofold axis, while the outer two water molecules (O32 and O32′ at pH 6.00) move closer to each other (Fig. 2).

At pH 5.00, the electron density shows the presence of the sulfate ion. As the pH increases, the occupancy of the sulfate ion at different pH values presents a decreasing trend (Table 3). At pH 6.98 and 9.00 a water molecule instead of the sulfate ion was modeled near the original sulfate position owing to the very weak density and the spherical shape of the peak (Fig. 2). The distances between the water molecules and the S atom of the sulfate ion at pH 5.00 are 1.24 Å at pH 6.98 and 2.12 Å at pH 9.00, respectively. The *B* factors were reasonable for a water molecule (44.76 Å^2 at pH 6.98 and 32.22 Å^2 at pH 9.00). Using the Bijvoet difference Fourier method (Strahs & Kraut, 1968), it may be determined whether the sites are water molecules or very low occupancy sulfate ions. Furthermore, the occupancy change of the sulfate ion may be monitored by the relative electron-density intensity of the S atom on Bijvoet difference Fourier maps.

3.2. Sulfate-binding region

The space group of the crystals is $I2_13$ and the unit-cell parameter is 78.70–78.87 Å. A threefold axis extends from the coordinate (0, 0, 0) to the coordinate (78.7, 78.7, 78.7). Three copies of Phe*B*1 from three symmetry-related insulin molecules are located around the threefold axis, about the coordinate (33.24, 33.24, 33.24) where a water molecule exists on the threefold axis (Fig. 4). Viewed down the threefold axis, the *B*-chain N-termini of three insulin molecules form the sides of depressions where three symmetry-related sulfate ions reside, each one occupying the space between two symmetry-related *B*1–*B*3 residues. The water molecule with a large *B* factor on the threefold axis is within hydrogen-bonding distance (2.6 Å) of three sulfate ions and three N atoms of three Phe*B*1 residues. The closest approach of the O atoms of the three symmetry-related sulfate ions is 4.4 Å and the sulfur-to-sulfur distance is 6.9 Å. The sulfate O atom nearest the threefold axis is coordinated by two symmetry-related *B*-chain N-terminal α-amino groups through hydrogen bonds of about 2.95 and 3.10 Å (pH $\leq$ 6.16) to form a nearly planar and hexagonal arrangement of atoms. The sulfate ion also forms hydrogen bonds with symmetry-related Val*B*2 and Asp*B*3 main-chain amides and one bound water (O28 at pH 5.00).

3.3. Interactions between Glu*B*13 and the sulfate ion

At pH $\leq$ 5.80, Glu*B*13 exists in conformation I and a water molecule (O33 at pH 5.80) forms a hydrogen bond with Glu*B*13 OE2 (Fig. 2). Through this water molecule and another one (O39 at pH 5.80), Glu*B*13 OE2 is linked to atom

Table 2
Comparison of porcine insulin structures at ten different pH values.

The root-mean-square difference (Å) between two compared structures for 394 non-H atoms is presented. Glu*B*13 is omitted in the comparison.

pH	5.00	5.53	5.80	6.00	6.16	6.26	6.35	6.50	6.98	9.00
5.00		0.137	0.238	0.262	0.274	0.301	0.312	0.296	0.306	0.465
5.53			0.248	0.277	0.286	0.308	0.327	0.311	0.306	0.471
5.80				0.168	0.170	0.229	0.253	0.267	0.282	0.436
6.00					0.174	0.225	0.205	0.227	0.269	0.417
6.16						0.249	0.247	0.257	0.260	0.426
6.26							0.123	0.141	0.210	0.394
6.35								0.143	0.207	0.391
6.50									0.182	0.375
6.98										0.382
9.00										

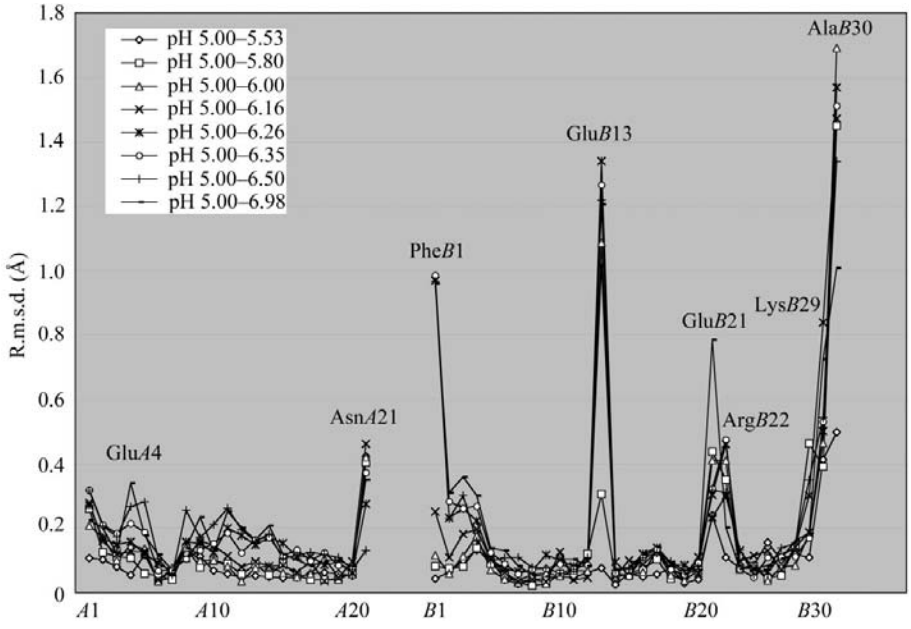

Figure 1
Root-mean-square differences between the structure at pH 5.00 and other structures at pH $\geq$ 5.53 as a function of residue number. The compared residues include *A*1–*A*21 and *B*1–*B*30, a total of 51 residues. Averaged coordinates for double conformations of Glu*B*13 (6.00 $\leq$ pH $\leq$ 6.98) are used in the comparison.

O1 of the sulfate ion. The sulfate ion is stabilized by the hydrogen-bonded interaction from these two water molecules, which have strong electron density. At pH $\geq$ 6.00, Glu*B*13 exhibits two conformations, I and II. Conformation II replaces the water molecule (O33 at pH 5.80) which hydrogen bonds with Glu*B*13 OE2 at pH $\leq$ 5.80. At pH $\geq$ 6.00, atom OE2 of conformation II of Glu*B*13 is bridged to atom O1 of the sulfate ion through only one water molecule (O39), which is located at almost the same position as O38 at pH 5.80. The *B* factors of the water molecule in the structures at pH 5.00, 5.53, 5.80, 6.00, 6.16, 6.26, 6.35 and 6.50 are 36.08, 44.06, 47.44, 51.14, 54.93, 58.86, 51.85 and 67.10 Å^2, respectively.

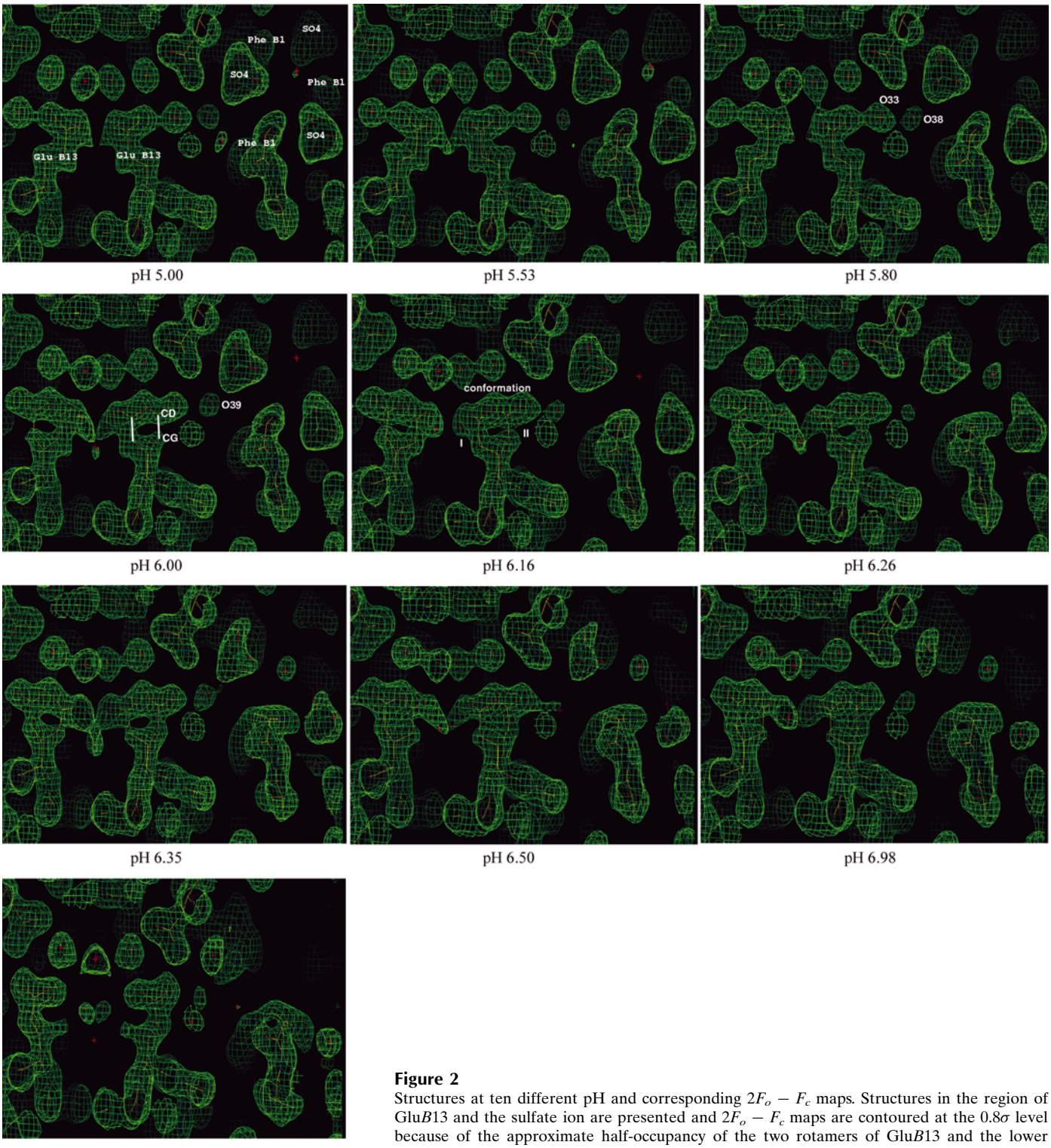

Figure 2
Structures at ten different pH and corresponding $2F_o - F_c$ maps. Structures in the region of Glu*B*13 and the sulfate ion are presented and $2F_o - F_c$ maps are contoured at the 0.8σ level because of the approximate half-occupancy of the two rotamers of Glu*B*13 and the lower electron density compared with the rest of the structure. Sub-figures correspond to the structures at pH 5.00, 5.53, 5.80, 6.00, 6.16, 6.26, 6.35, 6.50, 6.98 and 9.00, respectively.

3.4. The occupancies and electron density of Glu*B*13 and the sulfate ion

The occupancies of the two conformations of Glu*B*13 (Table 3) show that as the pH increases from 6.00 to 6.98, rotamers in conformation I switch to those in conformation II. Fig. 2 shows a subtle change of the electron density of Glu*B*13. At pH 6.00 the electron density for bond CG—CD of conformation II of Glu*B*13 is weaker than that for bond CG—CD of conformation I of Glu*B*13. At pH 6.16 and 6.26 the electron density for bond CG—CD of the two conformations of Glu*B*13 is almost equal. At pH 6.35 the electron density for bond CG—CD of conformation II of Glu*B*13 is stronger than that for bond CG—CD of conformation I. At pH 9.00 Glu*B*13 completes an evident switching from conformation I to conformation II.

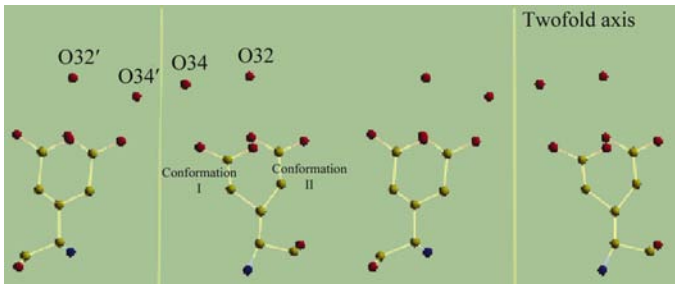

Figure 3
Stereoview of dyad-related double conformations of Glu*B*13 and water molecules. The coordinates at pH 6.00 were used to produce the figure.

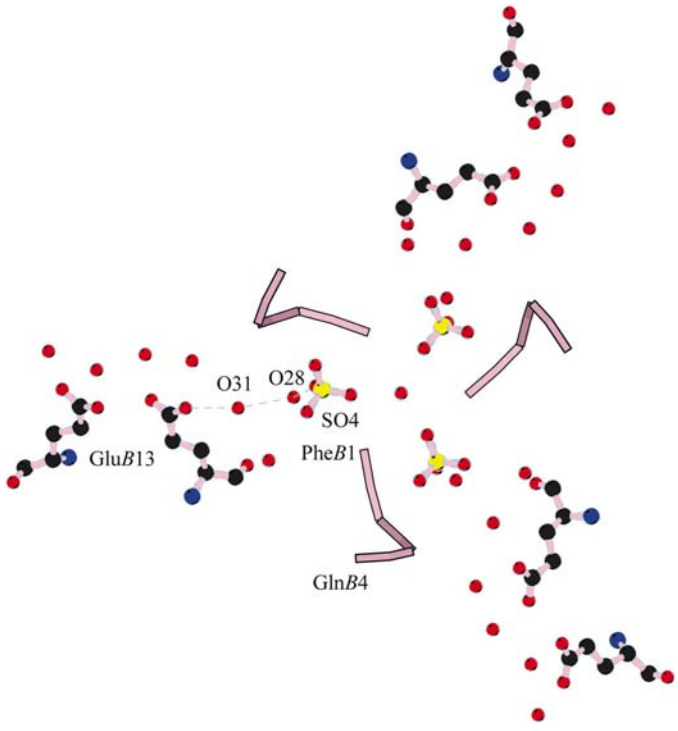

Figure 4
Sulfate-binding region. The coordinates at pH 5.00 were used to produce the figure.

Table 3
Occupancies of the sulfate ion and Glu*B*13 and *B* factors of Glu*B*13.

pH	SO_4^{2-}	Glu*B*13 q_1/q_2†	*B* factors‡
5.00	1.00	1.00/0.00	15.51
5.53	0.95	1.00/0.00	14.79
5.80	0.80	1.00/0.00	16.28
6.00	0.83	0.52/0.48	12.68
6.16	0.67	0.47/0.53	13.33
6.26	0.56	0.40/0.60	10.66
6.35	0.52	0.41/0.59	12.15
6.50	0.46	0.40/0.60	11.74
6.98	none	0.38/0.62	13.94
9.00	none	0.00/1.00	16.11

† q_1 and q_2 represent the occupancies of conformation I and conformation II of Glu*B*13, respectively. ‡ Averaged *B* factors of Glu*B*13.

The occupancy of the sulfate ion decreases gradually with increase in pH, except that the occupancy at pH 6.00 is a little abnormal and slightly higher than that at pH 5.80. The electron-density maps show that as the pH rises from 6.16 to 6.50, the electron density for the sulfate ion decreases.

3.5. Conformational change on Phe*B*1

Between pH 6.16 and 6.26, a significant conformational change occurs of Phe*B*1 (Figs. 5 and 2). N—CA—CB of Phe*B*1 rotates around the CA—C bond of Phe*B*1, although the aromatic ring on Phe*B*1 remains in almost the same position except for subtle rotation around its center of mass. At pH $\leq$ 6.16 the N—CA bond runs almost parallel to the threefold axis, whereas at pH $\geq$ 6.26 it lies almost in a plane perpendicular to the threefold axis. At pH $\leq$ 6.16 the NH_3^+ group of Phe*B*1 is located almost equally between the O atoms of two symmetry-related sulfate ions at 2.95 and 3.10 Å, respectively; at pH $\geq$ 6.26 the NH_3^+ group of Phe*B*1 is closer to an O atom of one sulfate ion (2.65 Å) than to the O atom of the other sulfate ion (4.08 Å). Three NH_3^+ groups of three symmetry-related Phe*B*1 residues are separated by 5.34 Å at pH 6.16, whereas after conformational change of Phe*B*1 the distance is 4.68 Å at pH 6.26. At pH 9.00 the whole residue Phe*B*1 has large shifts.

4. Discussion

4.1. Data and structure comparison

$R_{\rm merge}$ between pairs of data sets increases as the pH difference between them increases (Table 4). The first row of Table 4 shows a smooth gradient increase, suggesting that the porcine insulin structure changes gradually as a function of pH. Comparisons of calculated structure factors, calculated phases and map correlation coefficients produce similar results to those in Table 4, although the data do not change perfectly smoothly as do those in Table 4.

Table 2 shows a comparison of porcine insulin structures at different pH values. The overall structures are quite similar at all pH values, since the largest root-mean-square difference (r.m.s.d.) in atomic positions between any of the structures is

Table 4
Comparison of observed structure factors between data sets at different pH (R_{merge}).

$R_{merge} = \sum(||F_{o1}| - |F_{o2}||)/\sum(|F_{o1}|)$ for common reflections ($d < 10$ Å) between two data sets.

pH	5.00	5.53	5.80	6.00	6.16	6.26	6.35	6.50	6.98	9.00
5.00		5.36	7.05	7.16	10.44	10.50	12.82	14.32	16.47	26.69
5.53			6.95	6.97	9.48	11.43	11.92	13.59	15.75	25.53
5.80				6.33	8.29	9.00	9.45	10.97	13.21	24.13
6.00					6.83	8.82	8.76	11.12	12.79	23.24
6.16						7.20	6.74	8.73	10.18	21.07
6.26							5.70	6.66	9.19	21.08
6.35								6.33	7.93	20.17
6.50									7.49	19.35
6.98										15.48
9.00										

0.471 Å for 394 non-H atoms. However, the r.m.s.d. between pairs of structures increases steadily with the difference in pH. Although the values at pH 6.50 and 6.98 are perhaps slightly out of line, these values confirm that the porcine insulin structure changes gradually with pH.

The variations among the nine refined models are indicated by the r.m.s. differences in the atomic coordinates for each residue relative to the pH 5 model (Fig. 1). The models at different pH values generally appear to be superimposable. The largest differences, as expected, are in the coordinates of Phe*B*1 and Glu*B*13. Other residues which showed appreciable r.m.s. differences were Val*B*2, Asn*B*3 and Gln*B*4, whose movements are linked to the pH-dependent shift in Phe*B*1, and Gly*A*1, Glu*A*4, Gln*A*5, Asn*A*21, Glu*B*21, Arg*B*22, Pro*B*29 and Ala*B*30, which are surface-exposed residues whose positions may or may not vary systematically with pH. Excluding these eight flexible side chains and the five residues linked to pH-dependent transitions, the mean r.m.s.d. for the remaining 38 residues is 0.11 Å. This difference was comparable with the r.m.s.d. of 0.13 Å between the 42 well ordered residues of the pH 9 model in 1 *M* Na_2SO_4 refined in this study and the previously refined pH 9 model in 0.3 *M* Na_2HPO_4 (Badger *et al.*, 1991).

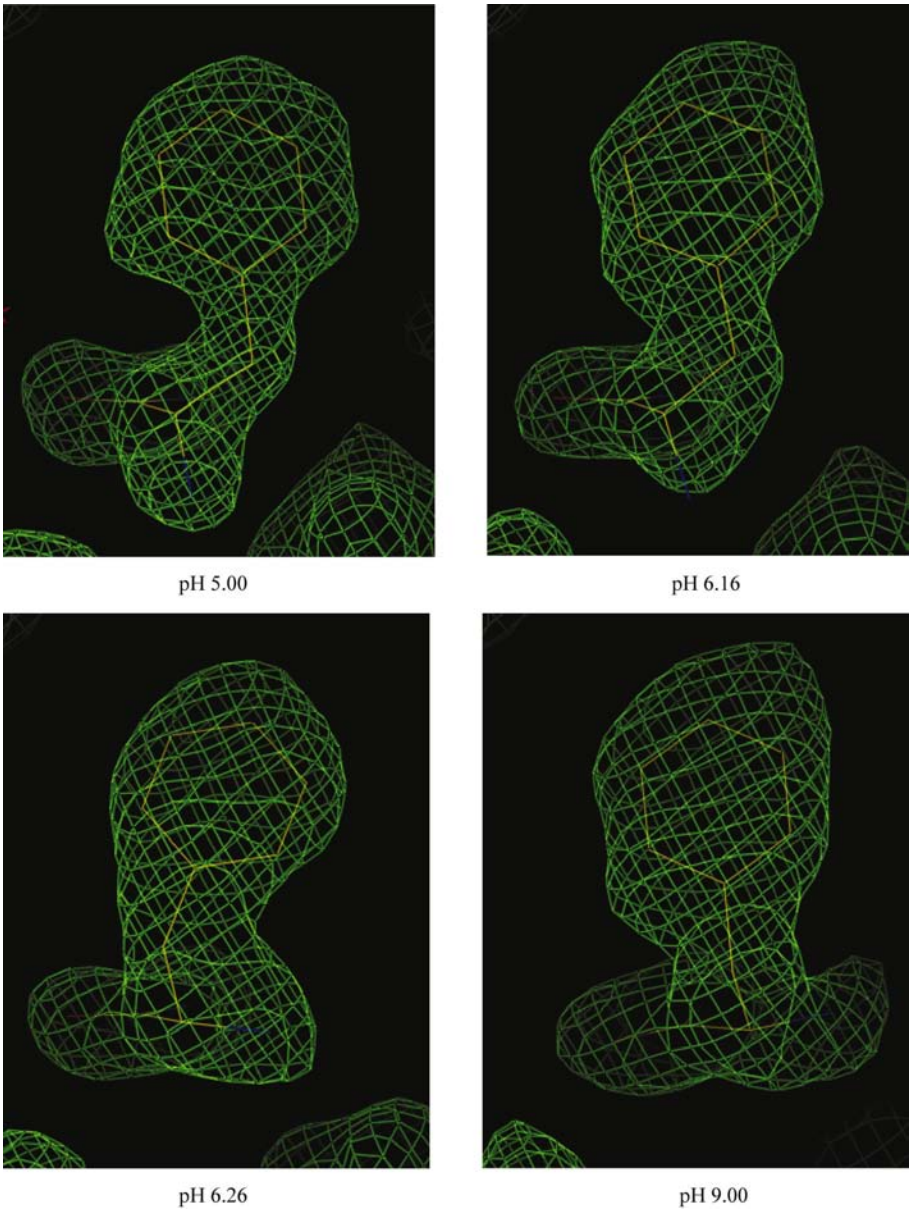

Figure 5
Conformational change of Phe*B*1. $2F_o - F_c$ maps are contoured at the 1σ level.

4.2. Glu*B*13 switching

At pH $\leq$ 5.80 the two Glu B13 residues interact across a crystallographic dyad, with the two carboxyl groups separated by only 2.78 Å. This close approach suggests that the pK_a of Glu*B*13 is higher than the normal pK_a of glutamic acid in solution (pK_a = 4.1). Electrostatic interactions between charged groups can cause pK_a shifts (Sørensen & Led, 1994) and in this case hydrogen bonding between the two carboxyl groups would be possible if at least one was protonated. Above pH 6.00 the Glu*B*13 side chain begins to change to conformation II, in which the carboxyl groups are further apart. This suggests that the change in conformation occurs to relieve electrostatic repulsion when the carboxyl groups are deprotonated. At pH 6.00 the occupancies of conformation I and II of Glu*B*13 are 0.52 and 0.48, respectively, and at pH 6.16 they are 0.47 and 0.53, respectively, suggesting that the pK_a may be around 6.08, where the occupancies would be equal.

4.3. The declining occupancy of the sulfate ion

Three symmetry-related sulfate ions are involved in electrostatic and hydrogen-bonded interaction with three $-NH_3^+$ groups from three symmetry-related Phe*B*1s. The occupancy of the sulfate ion decreases as pH increases. With distances between $-NH_3^+$ groups of 5.34 Å at pH 6.16 and 4.68 Å at pH 6.26, the electrostatic repulsion between the three $-NH_3^+$ groups may lower the pK_a of the $-NH_3^+$ group from its normal value (9.2). Therefore, an increase in pH may reduce the charge on the $-NH_3^+$ group, which impairs the electrostatic attraction between the $-NH_3^+$ group and the sulfate ion and destabilizes sulfate binding. Moreover, at pH $\geq$ 6.00 conformation II of Glu*B*13 replaces a water molecule which exists in structures at pH $\leq$ 5.80. Loss of this water molecule (O33 at pH 5.80) damages the hydrogen-bond network around the sulfate ion. Moreover, the change of Glu*B*13 to conformation II above pH 6.00 brings its carboxyl group closer to the sulfate position. Below pH 5.80 the distance between atom O1 of the sulfate ion and OE2 of conformation I of Glu*B*13 is 7.40 Å, whereas above pH 6.00 the distance of O1 from OE2 of conformation II is reduced to 5.10 Å. This suggests that the carboxyl group of conformation II of Glu*B*13 is involved in an electrostatic repulsion with the sulfate ion after Glu*B*13 switches from conformation I to conformation II. The electrostatic repulsion may impair sulfate-binding strength and lead to the decrease in the occupancy of the sulfate ion.

4.4. Conformational change on Phe*B*1

Between pH 6.16 and 6.26, Phe*B*1 makes an abrupt conformational change. Greater deprotonation of $-NH_3^+$ groups at pH 6.26 relieves the electrostatic repulsion among three symmetry-related $-NH_3^+$ groups, so that at pH 6.26 three $-NH_3^+$ groups can bear each other at a shorter distance of 4.68 Å, whereas at pH 6.16 the electrostatic repulsion keeps the three $-NH_3^+$ groups further apart (5.34 Å). Moreover, the declining occupancy of the sulfate ion and the deprotonation of the $-NH_3^+$ group suggest decreasing binding strength between the sulfate ion and the $-NH_3^+$ group. The impaired attraction force is unable to maintain the $-NH_3^+$ group to be located equally between two symmetry-related sulfate ions, so that N—CA—CB of Phe*B*1 rotates around bond CA—C at pH 6.26.

This work was supported by US Public Health Service grant CA 47439 from the National Cancer Institute to Professor Donald L. D. Caspar. The author thanks Dr Thayumanasamy Somasundaram for helping collect all the data. The author also thanks the reviewers for helpful suggestions.

References

Badger, J., Harris, M. R., Reynolds, C. D., Evans, A. C., Dodson, E. J., Dodson, G. G. & North, A. C. T. (1991). *Acta Cryst.* B**47**, 127–136.
Badger, J., Kapulsky, A., Gursky, O., Bhyravbhatla, B. & Caspar, D. L. D. (1994). *Biophys. J.* **66**, 286–292.
Brünger, A. T. (1992). *X-PLOR Version 3.1. A System for X-ray Crystallography and NMR.* Yale University, Connecticut, USA.
Collaborative Computational Project, Number 4 (1994). *Acta Cryst.* D**50**, 760–763.
Dodson, E. J., Dodson, G. G., Lewitova, A. & Sabesan, M. (1978). *J. Mol. Biol.* **125**, 387–396.
French, S. & Wilson, K. S. (1978). *Acta Cryst.* A**34**, 517–525.
Gursky, O., Badger, J., Li, Y. L. & Caspar, D. L. D. (1992). *Biophys. J.* **63**, 1210–1220.
Gursky, O., Fontano, E., Bhyravbhatla, B. & Caspar, D. L. D. (1994). *Proc. Natl Acad. Sci. USA*, **91**, 12388–12392.
Jones, T. A., Zou, J. Y., Cowan, S. W. & Kjeldgaard, M. (1991). *Acta Cryst.* A**47**, 110–119.
Otwinowski, Z. & Minor, W. (1997). *Methods Enzymol.* **276**, 307–326.
Sørensen, M. D. & Led, J. J. (1994). *Biochemistry*, **33**, 13727–13733.
Strahs, G. & Kraut, J. (1968). *J. Mol. Biol.* **35**, 503–512.
Yu, B. & Caspar, D. L. D. (1998). *Biophys. J.* **74**, 616–622.